Point-source-scattering from tyre-like structures above an impedance plane

Haike Brick[1], Martin Ochmann[1], Wolfgang Kropp[2]
[1] TFH Berlin - University of Applied Sciences, FB II, Computational Acoustics,
D-13353 Berlin, Germany, Email: brick@tfh-berlin.de
[2] Chalmers University of Technology, Division of Applied Acoustics, SE-41296 Gothenburg, Sweden

Introduction

In preceding publications [1, 2], we discussed the possibility to incorporate an infinite impedance plane into the direct Boundary-Element-Method (BEM) by means of an appropriate Green's function. This approach does not require a discretization of the impedance plane, since the Green's function fully takes into account the effects of reflection and absorption of the sound field caused by the impedance plane. The implementation was verified by analytical test cases for radiation problems. Now we focus on the scattering problem in presence of an impedance plane. The extension of the BEM-half space approach makes it possible to investigate the influence of the ground impedance on the well known horn effect of the tyre/road interface by means of BEM-simulations. The horn effect, an amplification mechanism of the horn-like geometry of the tyre/road interface, was experimentally investigated in a previous publications [3, 4]. These measurements serve as validation data for the BEM solutions. After a short review of the theory, we discuss the computational model, the numerical treatment of the complex horn-like geometry and the influence of a very soft impedance ground on the horn effect.

Theoretical background

The basis for the BEM is the Helmholtz-Integral-Equation (HIE), here for exterior scattering problems,

$$C(\vec{x})p(\vec{x}) = \int_{S_Q} \left(p(\vec{y}) \frac{\partial g(\vec{x},\vec{y})}{\partial \vec{n}_y} - \frac{\partial p(\vec{y})}{\partial \vec{n}_y} g(\vec{x},\vec{y}) \right) dS_y + p_{inc}(\vec{x}) \quad (1)$$

with

$$C(\vec{y}) = \begin{cases} 1 & \vec{x} \text{ in the exterior domain,} \\ \frac{1}{2} & \vec{x} \text{ on the surface } S_Q, \\ 0 & \vec{x} \text{ in the interior domain.} \end{cases}$$

The incident sound field p_{inc} is taken into account by an additional free term in the Helmholtz-Integral-Equation. In case of a half-space problem the total incident sound field p_{inc} consists of the direct wave from the source p_{src} and the wave, which is emitted by the source and scattered by the infinite plane p_p, that means $p_{inc} = p_{src} + p_p$ [5]. After discretising the surface S_Q into elements, a matrix equation for $p(\vec{x})$ is obtained

$$\mathbf{Cp} = \mathbf{Hp} + \mathrm{i}\,\omega \mathbf{Gv} + \mathbf{p}_{inc}, \quad (2)$$

in which $\mathbf{p}$ and $\mathbf{v}$ are the pressure and normal velocity at the surface elements and the matrices $\mathbf{H}$ and $\mathbf{G}$ contain the kernel functions $\partial g(\vec{x},\vec{y})/\partial \vec{n}_y$ and $g(\vec{x},\vec{y})$. The core of the HIE is the Green's function $g(\vec{x},\vec{y})$. As solution of the wave equation it describes the sound propagation between point $\vec{y} = (x_s, y_s, z_s)$ and point $\vec{x} = (x, y, z)$ and has to fulfil the boundary conditions on the surfaces S_Q and S_p (see Fig. 1) as well as Sommerfelds radiation condition at infinity. In case of a rigid infinite plane, the appropriate Green's function is

$$G(\vec{x},\vec{y}) = \frac{e^{-\mathrm{i}kR_1}}{4\pi R_1} + \frac{e^{-\mathrm{i}kR_2}}{4\pi R_2}, \quad (3)$$

with $k = \omega/c_0$, $R_1 = ||\vec{y} - \vec{x}||$ and $R_2 = ||\vec{y} - \vec{x}'||$. $\vec{x}'$ is the image of $\vec{x}$, mirrored by the infinite impedance plane. The time dependency $e^{\mathrm{i}\,\omega t}$ is omitted throughout the paper. Considering an arbitrary finite impedance boundary condition on the plane, a possible solution $G(\vec{x},\vec{y})$ is thoroughly discussed in [2] and [6]:

$$G(\vec{x},\vec{y}) = \frac{e^{-\mathrm{i}kR_1}}{4\pi R_1} + \frac{e^{-\mathrm{i}kR_2}}{4\pi R_2} + \frac{\mathrm{i}\gamma}{2\pi} \int_{-\infty}^{0} \frac{e^{-\mathrm{i}k\sqrt{\rho^2 + (z+z_s+\mathrm{i}\zeta)^2}}}{\sqrt{\rho^2 + (z+z_s+\mathrm{i}\zeta)^2}} e^{-\mathrm{i}\gamma\zeta} \mathrm{d}\zeta, \quad (4)$$

with $\rho = \sqrt{(x-x_s)^2 + (y-y_s)^2}$ as horizontal distance between $\vec{x}$ and $\vec{y}$. The complex quantity $\gamma = \Re\{\gamma\} + \mathrm{i}\,\Im\{\gamma\}$ follows from the plane's normalized impedance, $\gamma = \mathrm{i}k/Z_0$ with $Z_0 = Z/(\rho_0 c_0)$ and $\rho_0 c_0$ as impedance of the ambient fluid. Eq. (4) fulfils any arbitrary prescribed boundary condition on the plane and is appropriate to be implemented in a BEM code. The successful implementation of (4) in our in-house BEM-code BemLab was shown in [1] and [2] by means of various test cases.

Configuration

The investigated configuration is shown in Fig. 1. The horn effect is an amplification of the sound field radiated by sources close the the contact area of tyre and plane S_p at the field point $\vec{x}_{fp}$ [3]. The amplification is expressed as

$$\Delta L = 20 \log_{10} \left| \frac{p_{ts}(\vec{x}_{fp})}{p_s(\vec{x}_{fp})} \right|. \quad (5)$$

$p_{ts}(\vec{x}_{fp})$ represents the sound pressure at the field point in the presence of the tyre, $p_s(\vec{x}_{fp})$ is the field point sound pressure in the absence of the tyre. The horn's centre is

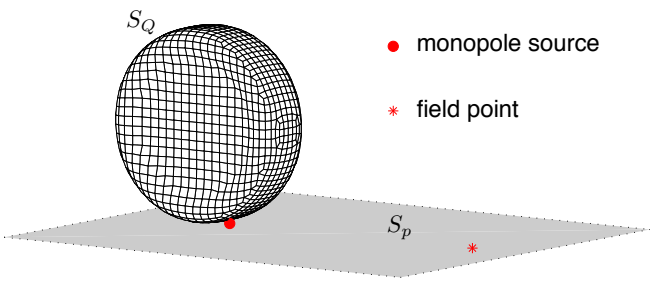

Figure 1: Position of tyre, monopole source and field point in the halfspace setting

located at the point of origin at (0, 0, 0). The source is a monopole source, located at the plane in a distance of 80 mm from the horn's centre at $\vec{y}_{scr} = (8 \cdot 10^{-2}\text{m}, 0, 0)$, its source strength is $A_{src} = 1$ N/m. The field point is placed at $\vec{x}_{fp} = (1\text{m}, 0, 0)$. The tyre is assumed to have a rigid boundary condition, i.e. the term $\partial p(\vec{y})/\partial \vec{n}_y$ vanishes on S_Q.

Tyre model

The tyre model does not have any tread pattern, a diameter of 62 cm and a width of 22 cm. In preliminary studies the most appropriate computational model was identified using LMS Sysnoise. A square and a rounded tyre model profile was tested, see Fig. 2, and the influence of a slight uplift of the tyre was investigated. The reference solution was the measured horn effect of the described configuration over rigid ground. A raise of the

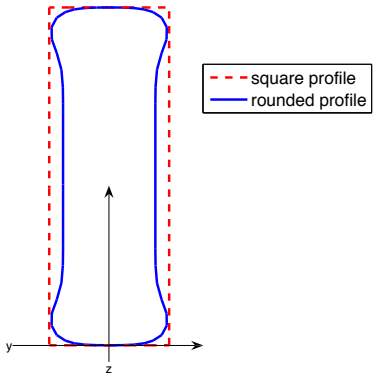

Figure 2: Cross section of the square and rounded tyre model

tyre is favourable in order to weaken the near-singularity of the integrand in (4), which occurs if both $\vec{x}$ and $\vec{y}$ are close to infinite plane, i.e. if the combined height $z + z_s$ is very small. As it is discussed in [3], the horn effect is very sensitive to any modifications of the horn geometry and the studies show the same effect. The influence of the configuration parameters can be seen in Fig. 3. The upper panel shows the strong influence of the height of the tyre over the plane. Only a few millimetres significantly change the amplification characteristic. For this study the square shaped tyre was used. The lower panel shows a comparison of the horn effect of the rounded and the square shaped tyre. The tyre with the square cross section leads to an overestimation of the amplification level ΔL. In this variation both types of tyres were raised by 1 mm. We decided to use the rounded tyre model, raised by 1 mm for our calculations.

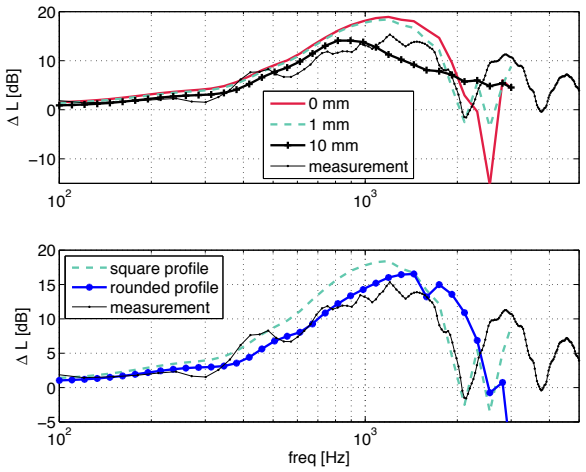

Figure 3: Amplification due to the horn effect for a tyre above a rigid plane. *Upper panel:* Dependence of ΔL on the heigth of the tyre over the rigid plane, *lower panel:* Dependence of ΔL on the profile of the tyre. Measurement data from [3].

Numerical treatment of the horn geometry

The BemLab-code uses a rough but fast one point integration for the evaluation of the discretised integral equation on S_Q. Considering the surface area close to plane, this approach is not sufficient, since in this area the "narrow gap" problem is encountered. Similar to the problem of very close boundary surfaces, such as narrow gaps or very thin structures, a near-singularity of the kernel functions occurs due a very small R_2 in the second term of (3) and (4). Our first approach was a refinement of this surface area until the element size matches the distance from its centre to the plane. The resulting tyre's surface mesh can be seen in Fig. 4. The figure shows

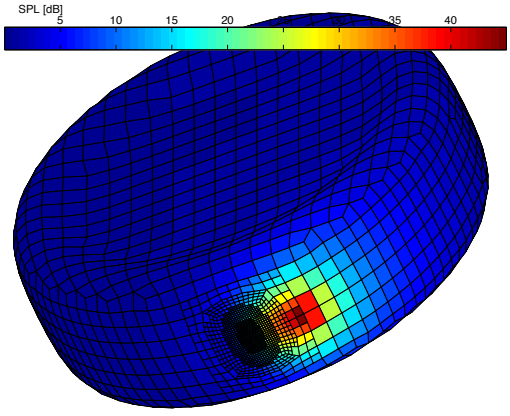

Figure 4: SPL on the refined surface mesh of the tyre at 985 Hz. The tyre is seen from the bottom.

the sound pressure level distribution (SPL) on the tyre's

surface at 985 Hz. Unfortunately, this approach leads to a doubling of the total number of elements. Second, we applied an *adapted* integration method, recently proposed in [7]. Each surface element is subdivided into intervals proportional to the relative distance between element's centre and plane. After assigning Gauss-Legendre integration points to the element subdivisions, the values of $g(\vec{x},\vec{y})$ and $\partial g(\vec{x},\vec{y})/\partial \vec{n}_y$ can be determined. The total number of elements remains the same as for the one-point-integration. The resulting distribution of integration points on the critical surface area of the tyre is shown in Fig. 5. While the finer mesh allows

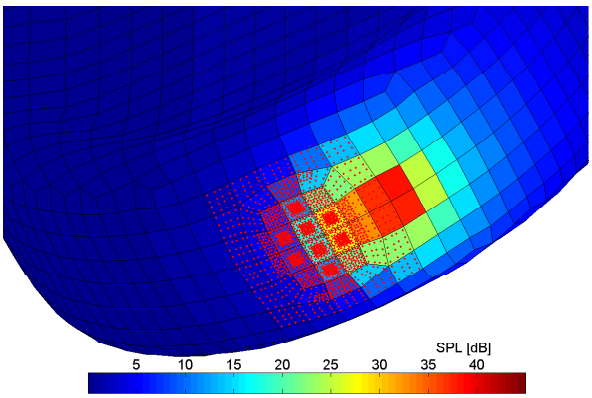

Figure 5: SPL on the surface mesh of the tyre at 985 Hz. The Gauss-Legendre integration points, resulting from the adapted integration method, are plotted as red points.

a higher resolution of the sound pressure distribution on the tyre's surface, the field point pressure in 1 m distance from the horn's centre can be modelled very well with both approaches as it is shown in Fig. 6. The resulting amplification level ΔL does not differ regarding the two methods, though the adapted integration method is considerably less time and memory consuming. In

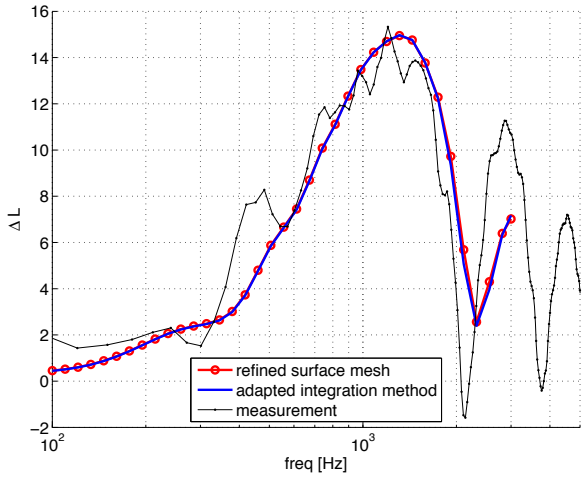

Figure 6: Amplification due to the horn effect of a tyre above rigid ground calculated with the refined tyre model and the adapted integration method on the basis of element subdivision. Measurement data from [3].

general, the computational results show an excellent agreement with the measured frequency response of ΔL.

Influence of the impedance plane

Considering (4) the most expensive step is the evaluation of the improper integral for every matrix coefficient of $\mathbf{H}$ and $\mathbf{G}$. For some configurations the very fast Gauss-Laguerre quadrature can be applied to solve the integral, otherwise an adaptive multilevel quadrature has to be used, which provides reliable results for all possible configurations, but is much slower [2]. The usage of the Gauss-Laguerre quadrature depends mainly on γ and the combined height of $\vec{x}$ and $\vec{y}$, $z + z_s$. Generally, the application of the Gauss-Laguerre quadrature is restricted to configurations with $\Im\{\gamma\} > 1$.

In the following, we choose a very soft rigidly-backed layer with an effective flow resistivity of $R_{eff} = 20$ kPas/m^2 as impedance plane. The height of the layer is 7 cm. Impedance and γ, respectively, of such a layer can be obtained by the impedance model of Delany&Bazley [8]. Fig. 7 shows the contour plot of necessary integration points of the Gauss-Laguerre quadrature depending on frequency and combined height $z + z_s$. As it can be seen, small heights of $\vec{x}$ and $\vec{y}$ and low frequencies are very unfavourable combinations regarding the application of the Gauss-Laguerre quadrature. In case, the number of integration points exceeds 100, the kernel functions have to be evaluated by the multilevel quadrature. The evaluation

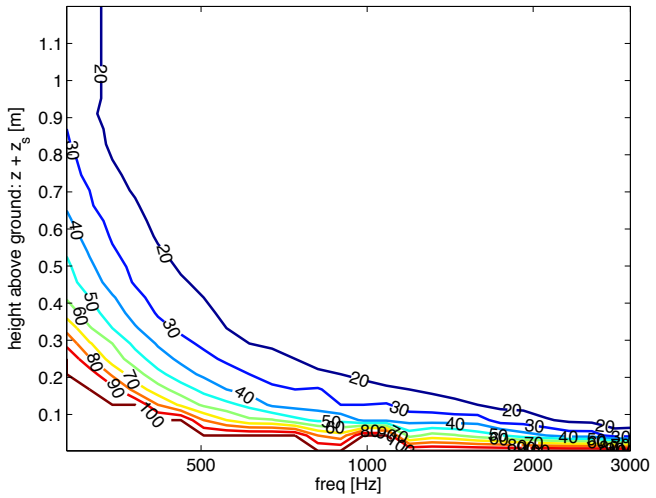

Figure 7: Contour plot of the necessary number of integration points to solve the integral in (4) by means of the Gauss-Laguerre quadrature depending on frequency and γ, respectively, and the combined height of $\vec{x}$ and $\vec{y}$.

of the matrix coefficients are the bottleneck of a BEM calculation including an impedance plane. While the calculation of one frequency step in case of a rigid plane takes around 0.3 minutes, it can take hours in case of a finite impedance of the ground.

Fig. 8 shows the resulting amplification due to the horn effect of a tyre above a rigid plane and above the soft impedance layer. The amplification levels ΔL differ significantly. In case of the impedance layer, the frequency of maximum amplification is shifted to lower frequencies and the total amplification level is dramati-

cally reduced. Above 1 kHz the frequency response of ΔL has a more rough characteristic. Either, the model starts to be numerically unstable or the roughness results from interferences of the sound field. This should be clarified by means of additional calculations with finer models.

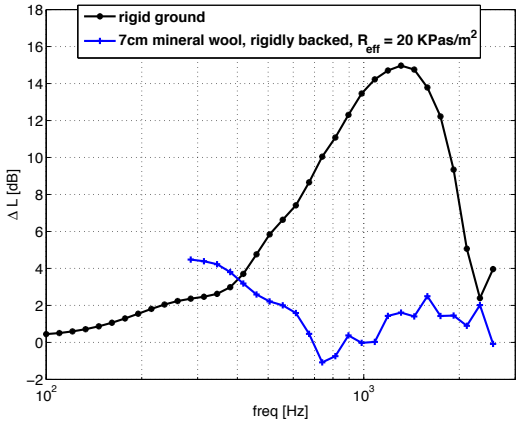

Figure 8: Amplification due to the horn effect of a tyre over rigid ground and over a very soft impedance layer

Fig. 9 shows the calculated and measured amplification ΔL for a slightly different configuration. The impedance plane is represented by a rigidly-backed mineral wool layer of thickness 1.6 cm and $R_{eff} = 124$ kPas/m^2. The tyre is raised by 1.85 cm. The source is located at $\vec{y}_{src}$=(18.2 cm, 0, 0) and the fieldpoint is at $\vec{x}_{fp}$ = (0.98 cm, 0, 19.7 cm). The predicted amplification

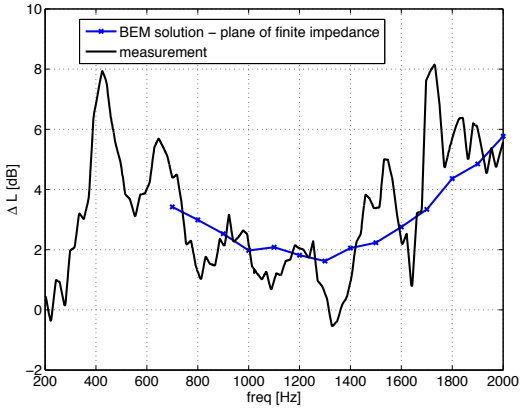

Figure 9: Calculated and measured horn effect of a tyre above an plane of finite impedance. Measurement from [4].

matches the measured frequency response very well. The measured curve shows more fluctuations but this might be due to a reverberant measurement environment or the finite size of the real mineral wool layer. The main amplification characteristic of the given setting can be modelled correctly. The calculation was limited towards the lower frequency range due to the increasing computational effort.

Summary

In this paper the influence of the impedance of an infinite plane on the horn effect was investigated by means of BEM-simulations. The horn-like geometry of the type/plane interface represents a geometrical and numerical complex situation. Since the horn effect is very sensitive to any geometrical modification, the tyre can not be lifted much without disturbing the effect. Close to the contact are of tyre and plane, the "narrow gap" problem is encountered, which requires a special numerical treatment. We have implemented successfully two approaches to handle the near-singularity of the kernel functions in the narrow gap area and have achieved an excellent agreement with measurement data for the case of a rigid ground. The evaluation of the kernel functions in presence of a plane of finite impedance is very time-consuming due to this difficult configuration. Nevertheless, we could show the strong influence of a very soft impedance layer on the horn effect. Additionally, a comparison with measured data shows a very high agreement with the calculated horn effect over an impedance plane. Hence, the extension of the BEM approach to half spaces with finite impedance boundary conditions is successfully validated by means of this scattering problem.

References

[1] H. Brick and M. Ochmann. A half-space BEM for the simulation of sound propagation above an impedance plane. In *Acoustics '08*, Paris, France, 2008.

[2] M. Ochmann and H. Brick. Acoustical radiation and scattering above an impedance plane. In S. Marburg and B. Nolte, editors, *Computational Acoustics of Noise Propagation in Fluids. Finite and Boundary Element Methods*, chapter 17, pages 459–494. Springer, Berlin, 2008.

[3] W. Kropp, F.-X. Bécot, and S. Barrelet. On the sound radiation from tyres. *Acta Acustica united with Acustica*, 86(5):769–779, 2000.

[4] F.-X. Bécot. *Tyre noise over impedance surfaces-Efficient application of the Equivalent Sources Method.* PhD thesis, Chalmers University of Technology, Gothenburg, Sweden & Insa – Scientific and Technical University, Lyon, France, 2003.

[5] A. F. Seybert and B. Soenarko. Radiation and scattering of acoustic waves from bodies of arbitrary shape in a three–dimensional half space. *Transaction of the ASME, Journal of vibration, acoustics, stress, and reliability in design*, 110(1):112–117, 1988.

[6] M. Ochmann. The complex equivalent source method for sound propagation over an impedance plane. *J. Acoust. Soc. Am.*, 116(6):3304–3311, 2004.

[7] V. Cutanda Henríquez and P. Juhl. Acoustic boundary element formulation with treatment of nearly singular integrands by element subdivision. In *19th International Congress on Acoustics - ICA 2007*, Madrid, Spain, 2007.

[8] M. E. Delany and E. N. Bazley. Acoustic properties of fibrous absorbent materials. *Applied Acoustics*, 3(2):105–116, 1970.